Physics of the Earth and Planetary Interiors 268 (2017) 54–64

Contents lists available at ScienceDirect

Physics of the Earth and Planetary Interiors

journal homepage: www.elsevier.com/locate/pepi

Present-day kinematics in the Eastern Mediterranean and Caucasus from dense GPS observations

Bahruz Ahadov [a,b,d], Shuanggen Jin [a,c,*]

[a] Shanghai Astronomical Observatory, Chinese Academy of Sciences, Shanghai 200030, China
[b] University of Chinese Academy of Sciences, Beijing 100049, China
[c] Department of Geomatics Engineering, Bulent Ecevity University, Zonguldak 67100, Turkey
[d] Institute of Geology and Geophysics, Azerbaijan National Academy of Sciences, Baku 1143, Azerbaijan

ARTICLE INFO

Article history:
Received 27 December 2016
Received in revised form 28 April 2017
Accepted 3 May 2017
Available online 10 May 2017

Keywords:
Tectonic activities
Strain rate
GPS
East Mediterranean
Caucasus

ABSTRACT

The Eastern Mediterranean and Caucasus are located among the Eurasian, African and Arabian plates, and tectonic activities are very complex. In this paper, the kinematics and strain distribution in these regions are determined and investigated from dense GPS observations with over 1000 stations and longer observations. The elastic block model is used to constrain present-day plate motions and crustal deformation. The relative Euler vectors between the Nubian, Arabian, Caucasus, Anatolian and Central Iranian plates are estimated. The Arabian-Eurasia, Anatolian-Eurasia, Nubian-Eurasia, Caucasus-Eurasia and Central Iranian Euler vectors are 0.584 ± 0.1 Myr^{-1}, 0.825 ± 0.064 Myr^{-1}, 0.35 ± 0.175 Myr^{-1}, 0.85 ± 0.086 Myr^{-1} and 0.126 ± 0.016 Myr^{-1}. The strain rate in the East Mediterranean and Caucasus has been estimated from the GPS velocity field. The results show that the thrust dominated areas, the eastern Mediterranean-Middle East-Caucasus and Zagros have negative dilatation and the western Anatolia region has positive 2D dilatation rate with significant rotation. The west Anatolian shows the extension in NW-SE with about 150–199 nstrain/yr in the W-E direction. The Central Anatolia shows compression rate below 50 nstrain/yr and extensional strain rate adjacent to East Anatolian Fault and Dead Sea Fault is about 0–100 nstrain/yr. The contraction strain rate is higher in Zagros and Caucasus between 100–150 nstrain/yr and contraction orientation is along the NE-SW direction in Caucasus. The north part of Iran shows less contraction rate below 50 nstrain/yr but North-East Zagros Mountains, Tabriz fault and Chalderan fault show extensional rate between 50–110 nstrain/yr and principal axes rotation in the N-S direction. The maximum contraction observed in the Kopek Dag is about 100–194 nstrain/yr and orientated in the NE-SW direction. East Zagros Mountain and Makran subduction zone have a large clockwise rotation with 70–85 nradian and principal axes remains mostly along the N-S direction. The observed extension is along N-S by about 0–100 nstrain/yr with counter clockwise rotation in Dead Sea Fault. The Sinai block shows shortening rate in the range of 0–100 nstrain/yr.

1. Introduction

The Eastern Mediterranean and Caucasus are located among the Eurasian, African and Arabian plates with complex tectonic activities, e.g., volcanic eruptions, mountain building and a large part of all earthquakes (Fig. 1) (McKenzie, 1972, 1978; Le Pichon and Angelier, 1979). The eastern Anatolian, the Caucasus, and the Bitlis-Zagros are active continental collision zones due to contemporary tectonic settings and structures. The Eastern Mediterranean is one of the important regions to understand the fundamental tectonic processes like continental rifting, passive margins, subduction and accretion, both collision and post collision (Robertson and Mountrakis, 2006). These general processes, in principle, are investigated for large areas of continental lithosphere to predict whether the region is aseismic and not deforming at present day. The plate tectonic perception provides a helpful description of continental deformation. In the Eastern part of the Anatolian block the plate motion is taken up by thrust faults associated with the Caucasus block. All the faults motion is approximately in the same direction as that of Arabia and Eurasia. The result of this geometry is that the continent, throughout the active region (McKenzie, 1972), continues to elevate the Caucasus. Eastern Mediterranean is centered on the interconnection of the Arabian with Eurasia and Anatolia plates towards the west from

* Corresponding author at: Shanghai Astronomical Observatory, Chinese Academy of Sciences, Shanghai 200030, China.
E-mail addresses: sgjin@shao.ac.cn, sg.jin@yahoo.com (S. Jin).

http://dx.doi.org/10.1016/j.pepi.2017.05.003
0031-9201/

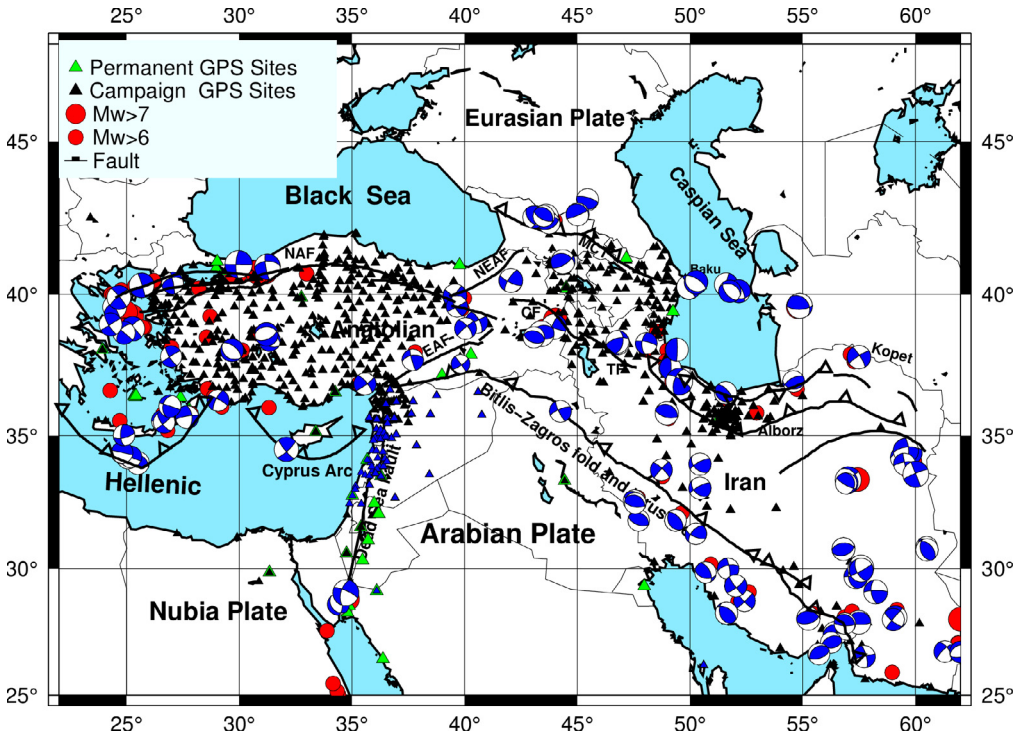

Fig. 1. Tectonics setting with main faults, earthquakes and GPS sites in East Mediterranean and Caucasus region. Focal mechanims of Mw ≥ 6 Earthquakes in this studied area are from Harvard Catalog (www.globalcmt.org/CMTsearch.html, 1976–2015). North Anatolian Fault (NAF), East Anatolian Fault (EAF), North East Anatolian Fault (NEAF), Main Caucasus Thrust (MCT), Chalderan Fault (CF), and Tabriz Fault (TF) are presented. Black lines faults and lines with triangle are thrust.

the most intense convergence zone. The collision of Saudi Arabia with Eurasia is reducing in the area of lithosphere within the deforming region. This reduction occurs with lateral transform of lithosphere by lithospheric shortening, supposedly associated with thickening of the captured lithosphere (e.g., McKenzie, 1972; Tenzer et al., 2015).

The Global Positioning System (GPS) has provided a new opportunity to directly observe the present day crustal motions and deformations as well as seismo-ionospheric disturbances (e.g., Hager et al., 1991; Afraimovich et al., 2010; Jin et al., 2007a, 2014, 2015). Previous GPS studies have helped to quantify regional deformation in the plate interaction zone (McClusky et al., 2003; Jin and Park, 2006; Jin et al. 2007b, 2013; Alchalbi et al., 2010; Le Pichon et al., 1995; Reilinger et al., 1997, 2006; Vernant and Chéry, 2006; Nyst and Thatcher, 2004; Mahmoud et al., 2005; Aktug et al., 2009; Aktuğ et al., 2013a,b). The regional plate motion studies use the fault orientation, local observations and constraints from the relative plate motion. The Eastern Mediterranean region experienced many destructive earthquakes throughout its recorded history. The earthquake activity observed around the Aegean Sea comprising a large part of Greece and Western Anatolia has been the most remarkable geodynamics phenomenon in the Eastern Mediterranean region. The tectonic evolution of the Eastern Mediterranean region is dominated by the effects of subduction along the Hellenic (Aegean) arc and of continental collision in eastern Turkey (Anatolia) and the Caucasus. Northward subduction of the African plate, western Turkey and the Aegean region is an extension of the continental crust (McClusky et al., 2000, 2003). In terms of historical seismicity, large earthquakes have been occurred with magnitudes greater than (M_w) 6 in East Mediterranean and Caucasus. The Anatolia plate has been of interest for more than two decades of GPS studies, mostly concentrated on the seismical and tectonic active Marmara region, Western Anatolia, Central Anatolia and North Anatolian Fault System with determining the strain and slip rates (Reilinger et al., 1997; Aktuğ et al., 2013a,b). However, detailed deformation and active tectonics in these areas are still not clear due to short time observations and limted stations.

In this paper, more than 1000 continuous GPS (CGPS) and survey-mode GPS (SGPS) stations velocity field with longer observations is collected to study the spatial distribution of present-day crustal deformation and tectonic plate motion in the eastern Mediterranean and Caucasus regions. In Section 2, tectonics setting is introduced, dense GPS-derived velocity field collected from recent studies is presented in Section 3, the kinematic results of continental deformation in the Eastern Mediterranean and Caucasus region are presented and discussed in Section 4, and finally the conclusions are given in Section 5.

2. Tectonic setting

The eastern Mediterranean is the favorable place to investigate plate tectonics with three major tectonic plates, Arabia, Nubia, and Eurasia. The Caucasus is located in continental collision zone between Arabia and Eurasia between the Black and the Caspian Sea. The oceanic collision occurs in the Hellenic and Cyprian Arcs between Nubia and Anatolian as a subduction. As a result, the Arabian plate is separating from the Sinai sub-plate with the Dead Sea Fault (DSF) transform plate boundary. Seismic activity is distributed over a wide area in the North of the Dead Sea, reflecting spreading out deformation in northern Israel and Lebanon.

Arabia-Nubia divergent motion in the Red Sea into the convergence motion between Eurasia and Arabia is currently expressed by extrusion of Anatolia. However, not all the African-Arabian divergent motion is transferred (Wdowinski et al., 2004) northward to the convergence zones. The southwestern boundary between Nubia and Sinai of the divergent motion in the Red Sea propagates into the Gulf of Suez. Extensive variety exists the tectonic development in the Anatolia and the surrounding regions

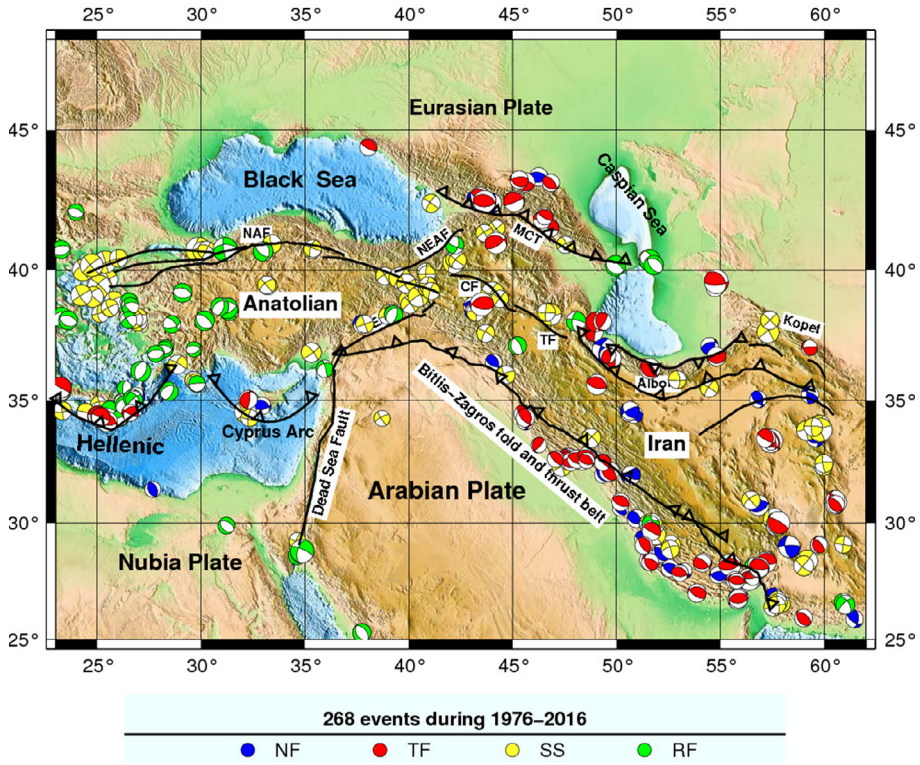

Fig. 2. Tectonic regimes obtained from the sum of moment tensors (http://ds.iris.edu/spud/momenttensor) with hypocentral depths ≤35 km.

(Fig. 2), the transform strike-slip faulting (North and East Anatolia Faults), continental collision and major thrust faulting (Bitlis-Zagros, Caucasus), subduction (Nubia, Arabia), contraction (Caucasus, Marmara Sea), extension (Western Anatolia) and many relatively small displacements (McKenzie, 1972; Jackson and McKenzie, 1984; Barka and Reilinger, 1997). Anatolia is the result of the interaction between Arabian and African Plates with Eurasia (McKenzie, 1972; Jackson and McKenzie, 1984). The Caucasus moves on the northern belt of the Alborz Mountain and joins the northernmost belt in the Kopet Dag. The southernmost belt follows the Zagros range close to the northern boundary of the Arabian Plate. All three boundaries show thrusting due to Centroid Moment Tensor solution (Fig. 2). The strike-slip components for main shocks cannot be determined because most of the targets are in the crust. The seismic activity in Turkey is different from Iran because big earthquakes occurred in regions far from the three belts. The North Anatolian Fault is often not produced by the slip, even when the shocks are within the belts (McKenzie, 1972). The Dead Sea Transform Fault is characterised by left-lateral motion due predominantly to tectonic motion between Africa and Arabia. The Bitlis-Zagros fold and thrust belt of northward motion result in a continental collision. Eastern Turkey, the Caucasus Mountain and westward extrusion of the Anatolian plate are observed with earthquake activity and high topography (McKenzie, 1970).

The Anatolian block is almost rigid block deformation. The North Anatolian fault, the slip rate is 25 mm/yr, defining a major boundary separating the motion of Anatolia from Eurasia, with slow deformation in the central Anatolian (McClusky et al., 2000). The distribution of earthquakes indicates that the crust is undergoing active deformation in the western Turkey. According to Nyst and Thatcher (2004) and Reilinger et al. (2006) GPS velocity in western Turkey accomplished a small number of rigid blocks.

Due to the northward motion of Arabian Plate along Bitlis-Zagros suture zone (Koçyiğit and Erol, 2001), Eastern Anatolia is characterised by shortening and Western Anatolia is by extension under a north-south orientation driven by subduction in Hellenic Trench. Central Anatolia is a wedge-shaped structure with relatively low seismicity and less internal deformation surrounded in the East by sinistral East Anatolian Fault System (EAF) and in the North by dextral North Anatolian Fault (NAF) (Jackson and McKenzie, 1984; Taymaz et al., 1991; Barka and Kadinsky-Cade, 1988; Aktuğ et al., 2013a,b).

According to GPS velocities results, the kinematics of the northern DSFS deviated significantly from plate tectonic predictions models that the Sinai and Arabian plates were considered as a rigid (Reilinger et al., 2006). Sinai and Arabian plates actively converge with the Eurasia plate. The Zagros mountain belt is approximately 1500 km long, 250–400 km wide and extends from eastern Turkey (Tatar et al., 2002) to the Oman Gulf, where it ends at the Makran subduction zone. The Zagros accommodates part of the convergence between Arabia and Eurasia. The NUVEL1A model (DeMets et al., 1994) predicted an N-S shortening with 30–40 mm/yr between Eurasia and Arabia, and Bitlis-Zagros confine relative motion between the Africa, Arabia, and Eurasia.

3. Data and methods

In this paper, a dense GPS-derived velocity field is collected and transferred into the consistent Eurasian plate fixed reference frame from recent studies (Alchalbi et al., 2010; Kadirov et al., 2014; Reilinger et al., 2006; Aktug et al., 2009; Aktuğ et al. (2013a,b); Mahmoud et al., 2013; Karakhanyan et al., 2013; Masson et al., 2007; Djamour et al., 2010; Bayer et al., 2006). All GPS data have at least five years of observations. Fig. 3 shows GPS velocities at 1153 stations with survey-mode GPS (SGPS), continuous GPS (CGPS) and IGS stations.

In Figs. 3 GPS velocities are shown in a Eurasia fixed reference frame with 2σ error ellipse of 95% confidence ellipses using the GAMIT/GLOBK software (King and Bock, 2004; Herring et al.,

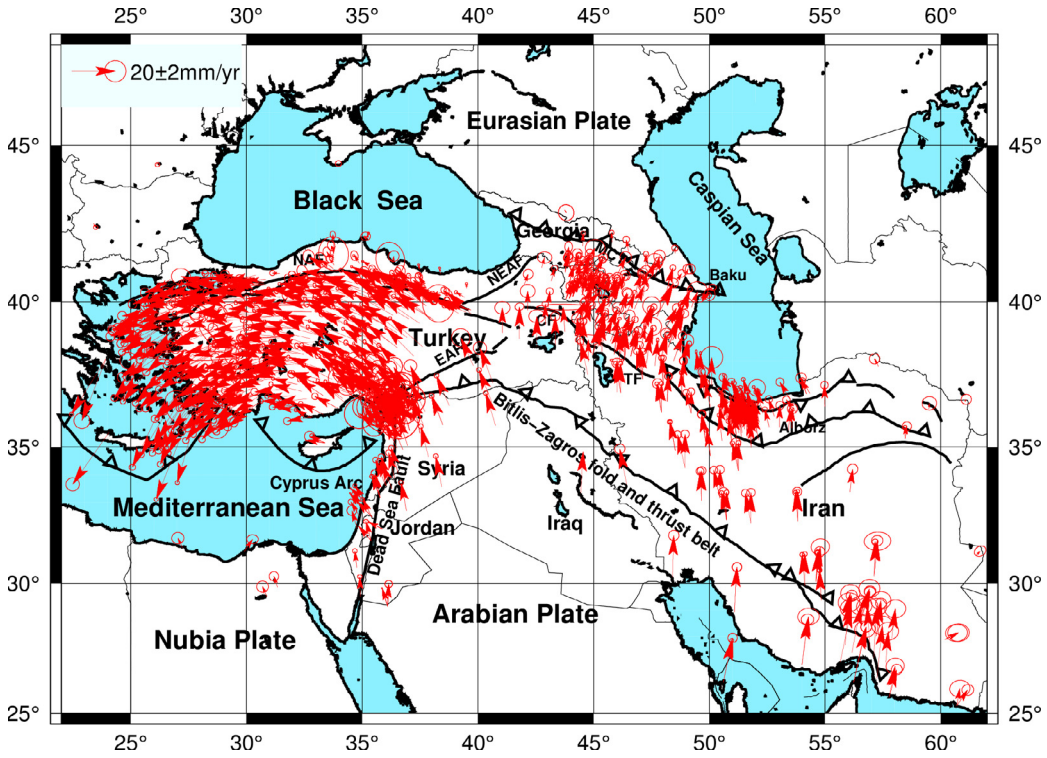

Fig. 3. GPS velocities with 95% confidence ellipses in a Eurasia fixed reference frame. North Anatolian Fault (NAF), East Anatolian Fault (EAF), North East Anatolian Fault (NEAF), Main Caucasus Thrust (MCT), Caucasus Fault (CF), and Tabriz Fault (TF) are marked. Black lines faults and lines with triangle are thrust faults.

2006). The motions of plates on the Earth surface can be described by Euler rotations. The motion of any spherical plate can be expressed by a single rotation about a suitably chosen axis which passes through the center of the Earth. The intersection of the rotation axis with the Earth's surface is called Euler pole. The mathematical foundation for rotations on a sphere is Euler's theorem. Therefore, the motion of plates can be described by simple rotations with the assumption of rigid plates on a spherical Earth. According to the Euler theorem for a rigid block, the block kinematic model can be defined by the following equation (DeMets et.al., 1990):

$$v_j = \Omega x r_j \tag{1}$$

where r and v are the position and velocity vectors at j_{th}, respectively, and Ω is the Euler rotation vector. Eq. (1) can be rewritten in the following matrix form:

$$\begin{bmatrix} v_n \\ v_e \end{bmatrix} = \begin{bmatrix} r\sin\lambda & -r\cos\lambda & 0 \\ -r\sin\varphi\cos\lambda & -r\sin\varphi\sin\lambda & r\cos\varphi \end{bmatrix} \begin{bmatrix} \Omega_x \\ \Omega_y \\ \Omega_z \end{bmatrix} \tag{2}$$

where (λ, φ) are the longitude and latitude of any point in a block, V_e and V_n are the eastern and northern components of the velocity vector, r is the Earth radius, and Ω_x, Ω_y, Ω_z are the components of the Euler vector.

Using more than two stations for each block, we can estimate Euler parameters using weighted least squares algorithm from Eq. (2)

$$\Omega = \sqrt{\Omega_x^2 + \Omega_y^2 + \Omega_z^2} \quad \beta = tg^{-1}\frac{\Omega}{\sqrt{\Omega_x^2 + \Omega_y^2}} \quad \alpha = tg^{-1}\frac{\Omega_y}{\Omega_x} \tag{3}$$

where β and α are the Euler rotation latitude and longitude, respectively.

In regional deformation studies, it is important to determine the strain rate. The segment approach divides the target area into a number of grids to compute the individual strain field for each grid. Another approach, called Gridded method (Shen et al., 1996), involves to computing the partial derivatives of strain field for individual grid points. The Grid approach interpolates using geodetic measurements for the strain rates calculation. At each location, a uniform strain rate field is assumed, and a least squares inversion is performed over the station velocity solutions to solve for six parameters: the velocity components U_x and U_y rotation rate ω and strain rate components ε_{xx}, ε_{xy} and ε_{yy}. The modelling parameters can be written from Shen et al. (1996) as:

$$\begin{pmatrix} V_e^l \\ V_n^l \end{pmatrix} = \begin{pmatrix} 1 & 0 & \Delta x_i & \Delta y_{i_i^j} & 0 & \Delta y_i \\ 0 & 1 & 0 & \Delta x_i & \Delta y_i & -\Delta x_i \end{pmatrix} \begin{bmatrix} U_x \\ U_y \\ \tau_{xx} \\ \tau_{xy} \\ \tau_{yy} \\ \omega \end{bmatrix} + \begin{pmatrix} \varepsilon_x^l \\ \varepsilon_y^l \end{pmatrix} \tag{4}$$

where V_e^l and V_n^l are the station velocities at I_{th}. All variables on the Eq. (4) are evaluated at a location $\vec{R}$, Δx_i and Δy_i are the vector components, ε_x^l and ε_y^l are the errors of the appropriate velocity components. The covariance matrix for ε_x^l and ε_y^l is E_{ij}, and C_{ij} is the covariance matrix of the velocity estimation errors obtained from GPS data arrangement. The weighted E_{ij} can be written as following equation:

$$E_{ij} = C_{ij}\exp\frac{\Delta R_i^2 + \Delta R_j^2}{\sigma_D^2} \tag{5}$$

where i and j are the velocity components and corresponding to i_{th} and j_{th} stations, ΔR_i and ΔR_j are the distances and σ_D is a distance-decaying constant. The 2D dilatation for each point is calculated by

$$\Delta = \tau_{xx} + \tau_{yy} \tag{6}$$

The gridded technique can either use the nearest neighbor or a distance weighted approach. In both cases, a uniform grid is constructed for the study area and calculates the velocity gradients for each grid node. These methods mainly differ depending upon how a station is chosen for the analysis of each node. In this study the distance weighted method has been chosen, i.e., the velocity gradients have been calculated from more than three stations closest to each node.

4. Results and discussion

4.1. Rigid block motions

In Fig. 3 the GPS velocity field shows the counterclockwise rotation of most central and western Turkey due to northward motion of Africa plate and northwest motion of Arabian plate. This rotation is surrounded by the NAF and extends to the north Aegean Sea. Motions in eastern Turkey show progressively east directions toward the NNE, resulting in shortening of the Caucasus thrust into Armenia and Georgia. The Lesser Caucasus and Kura Basin cannot be explained well with the Arabian push and a slab pulls under the Caucasus and the Apsheron-Balkan Sill, which is likely to occur (Vernant and Chéry, 2006). Active continental collision in eastern Turkey and the Lesser Caucasus is causing the lateral transport (Reilinger et al., 2006) of lithosphere out of the zone of plate convergence and shortening along the Main Caucasus Thrust. In addition, the boundary between the Arabian plate and the Anatolian plate is characterised by predominantly left-lateral strike-slip motion without fault-normal convergence and a small amount of extension. Aktuğ et al. (2013a,b) estimated a Euler Pole for Anatolia–Eurasia motion without simultaneously estimating translation rate of angular velocity (1.380 ± 0.01). McClusky et al. (2000) and Reilinger et al. (2006) concluded that the kinematics of the Eastern Mediterranean and Caucasus can be modelled by the rigid body relative rotation of a small number of blocks. We use the same block model to estimate the rotation vectors for each block. The block boundaries are determined from faults, seismicity, and historical earthquakes. We applied an approach similar to McCaffrey (2002), where all the Euler rotations of the micro blocks are simultaneously estimated by minimizing the residual of the velocities. Euler vectors have been determined from GPS data for the Nubian, Arabian, Anatolian and Caucasus plates including small blocks with respect to Eurasia plate (Table 1). Relative motion derived from the GPS-estimated Euler vectors along plate boundaries is shown in Fig. 4.

The anticlockwise rotations of Anatolia with respect to Eurasia in terms of Euler vector are observed. Fig. 5 shows residual velocities at all GPS stations after removing the rigid plate motions. Relative block motions at the plate boundaries (relative Euler vectors, Table 1) are solved by minimizing the GPS residual motions (Fig. 5) within the blocks using the least squares.

WRMS residuals for each plate/block are given in Table 1. The block model provides a good fit to the observations overall, and a number of areas show significant residual deformation motions. Maximum residual motions are observed in western Turkey. Larger residual velocities are found especially in block boundaries.

Table 1
GPS-estimated Euler vectors relative to Eurasia plate with 1σ uncertainties.

Blocks	Longitude E	Latitude N	Rate, deg/Myr	σ	WRMS, mm/yr	Number of stations	References
CI-EU	−20.7	7.84	0.126	0.016	2.49	75	This Study
CI-EU	4.2	18.9	0.207	0.02			Reilinger et al. (2006)
CI-EU	−13.6	4.2	0.149	0.007			Djamour et al. (2010)
CA-EU	38.09	43.5	0.85	0.086	8.67	141	This Study
CA-EU	37.8	42.1	0.84	0.06			Reilinger et al. (2006)
BS-EU	48.41	−44.5	0.149	0.041	1.82	19	This Study
BS-EU	31.4	43.3	0.231	0.01			Reilinger et al. (2006)
AL-EU	6.087	19.55	−0.149	0.047	1.73	57	This Study
AL-EU	57.9	36.6	−1.299	0.79			Reilinger et al. (2006)
AL-EU	59.4	0.70	−0.969	0.072			Djamour et al. (2010)
KA-EU	69.12	−30.3	−0.378	0.126	1.60	20	This Study
KA-EU	81.5	29.4	−0.225	0.124			Reilinger et al. (2006)
KA-EU	64.3	0.10	−0.61	0.024			Djamour et al. (2010)
AN-EU	30.22	28.53	0.825	0.064	3.84	233	This Study
AN-EU	32.1	30.8	1.231	0.023			Reilinger et al. (2006)
AN-EU	32.6	30.8	1.20	0.10			McClusky et al. (2000)
AN-EU	14.6	34.0	0.64				Jackson and McKenzie (1984)
AN-EU	31.0	35.5	0.83	0.10			Westaway (1994)
AN-EU	31.96	32.02	1.307				Le Pichon and Kreemer (2010)
LU-EU	70.73	−14.7	−0.98	0.40	3.57	9	This Study
LU-EU	83.2	26.1	−0.152	0.079			Reilinger et al. (2006)
AR-EU	31.4	12.0	0.485				DeMets et al. (2010)
AR-EU	23.02	29.03	0.584	0.10	3.10	63	This Study
AR-EU	18.4	28.4	0.428	0.009			Reilinger et al. (2006)
AR-EU	18.4	27.4	0.4	0.04			McClusky et al. (2003)
AR-EU	19.5	27.9	0.41	0.10			Vernant et al. (2004)
AR-EU	15.21	28.31	0.396				Le Pichon and Kreemer (2010)
SIN-EU	10.68	13.6	0.154	0.03	2.39	52	This Study
SIN-EU	−19.1	1.80	0.088	0.041			Reilinger et al. (2006)
SIN-EU	16.62	23.14	0.2242	0.147			Wdowinski et al. (2004)
SWAN-EU	32.02	35.66	2.801	0.770	2.05	18	This Study
SWAN-EU	32.2	34.5	3.774	0.238			Reilinger et al. (2006)
AG-EU	41.65	29.29	0.922	0.266	3.27	12	This Study
AG-EU	52.3	15.9	0.563	0.028			Reilinger et al. (2006)
MAR-EU	23.99	−46.7	1.822	0.42	5.85	26	This Study
MAR-EU	28.4	35.1	2.370	0.106			Reilinger et al. (2006)
NU-EU	21.6	−20.4	0.131				DeMets et al. (2010)
NU-EU	35.42	−31.2	0.350	0.175	2.61	4	This Study
NU-EU	−23.9	−2.30	0.059	0.001	1.29		Reilinger et al. (2006)

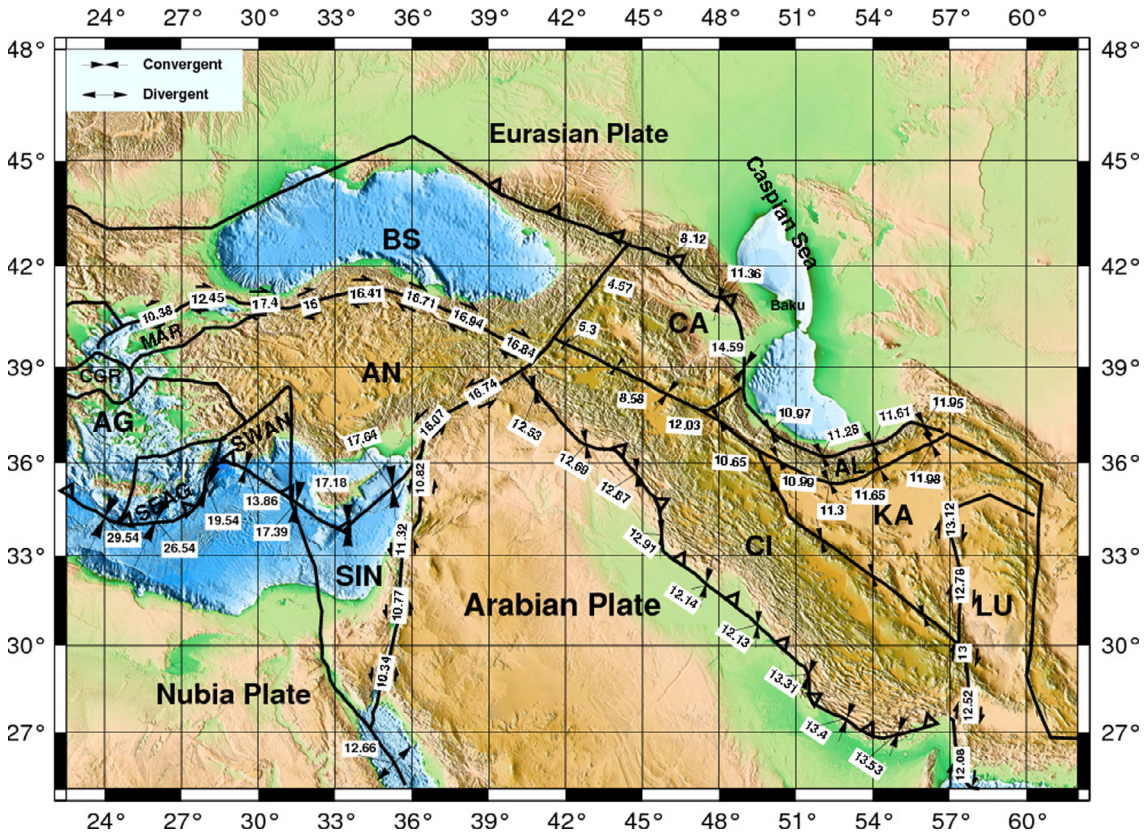

Fig. 4. Relative motions at plate boundaries in the Eastern Mediterranean and Caucasus derived from the Euler vectors determined in this study.

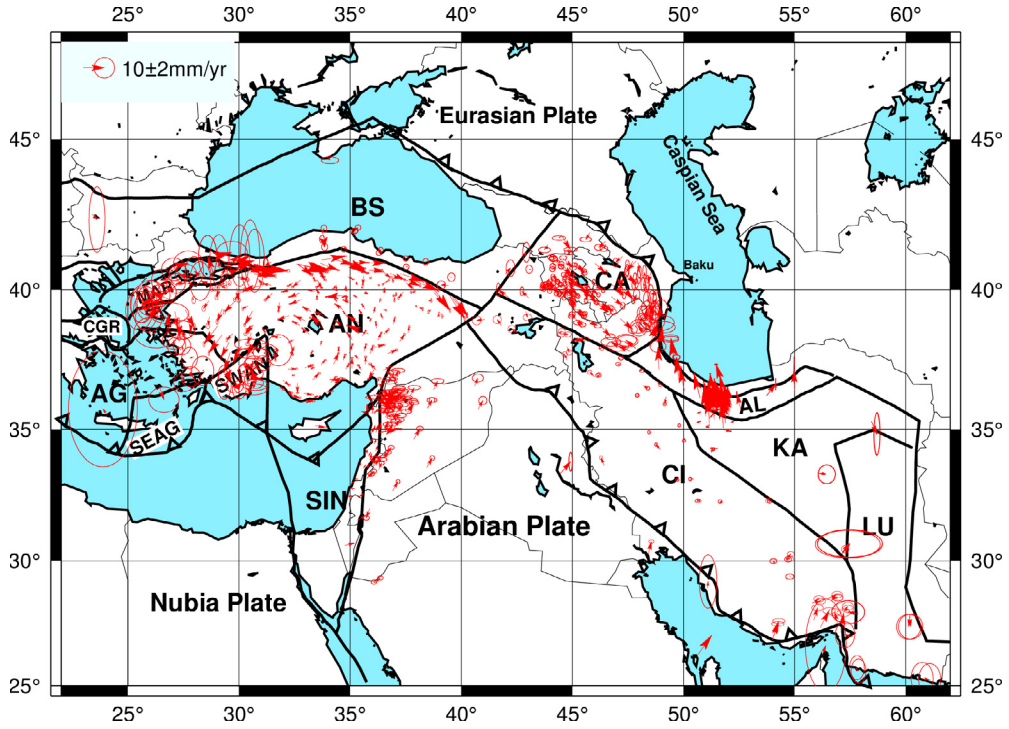

Fig. 5. Residual velocities with 95% confidence ellipses for the block model. Residuals for stations from the Euler vectors.

We use a simple plate boundary model to investigate deformation within the plate boundary zones. This model allows us to investigate the total deformation being accommodated within these areas and provides the plate boundary conditions (McClusky et al., 2003).

The angular velocity field shows counterclockwise and clockwise rotation. The Counterclockwise rotation is located on the Arabian plate, Anatolian plate, Caucasus block and Central Iranian block. Clockwise rotations are located in Kavir, Alborz and Lut. We have compared our results with other related studies (as

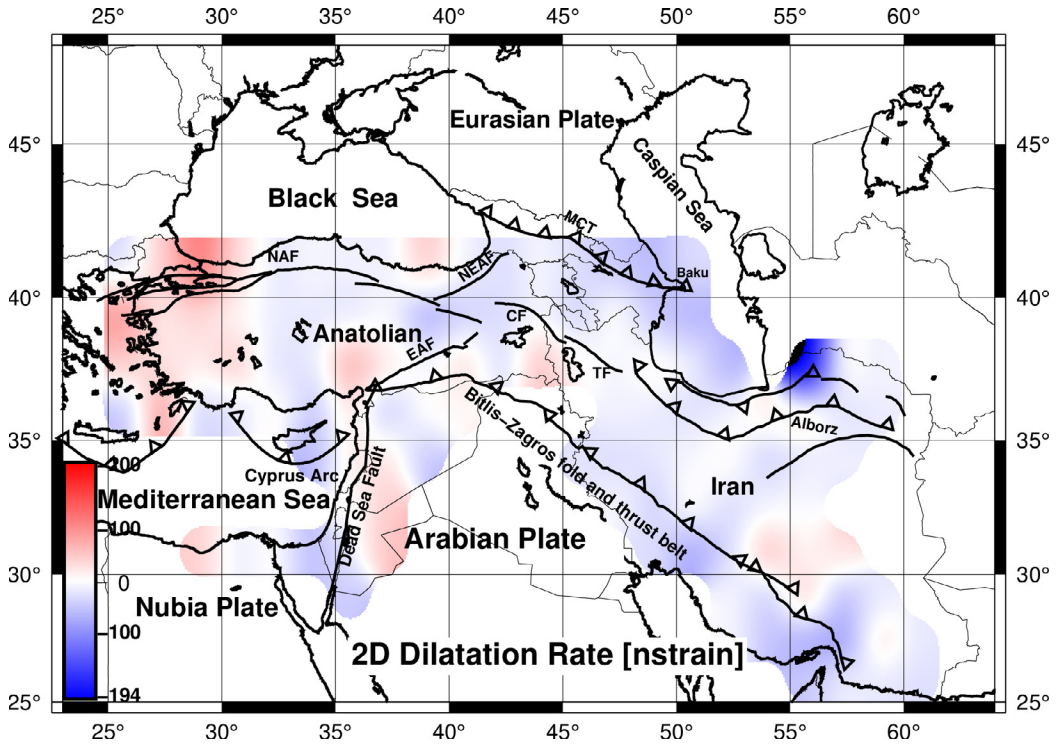

Fig. 6. Map of the magnitude of two dimensional dilatation rates in the East Mediterranean and Caucasus calculated from the GPS vectors. Red is positive and blue negative.

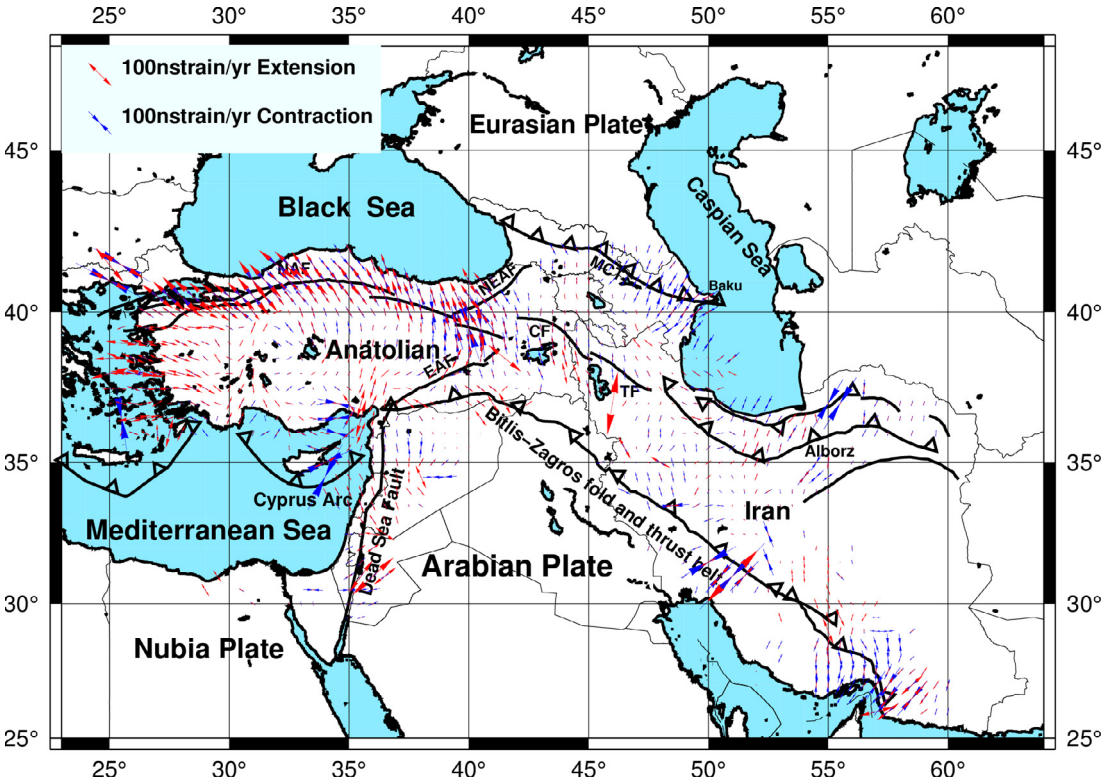

Fig. 7. The principal horizontal axes of the strain rate tensors in East Mediterranean and Caucasus. The red arrows are extension strain rate and the blue arrows contraction strain rate. The convergent arrows are contraction and the divergent arrows are extension.

shown in Table 1) and our angular velocities are comparable to them. Our results for orientation of relative motion agree with predicted GPS velocities. The estimated relative motions along the block boundaries are shown in Fig. 4, where arrows denote the transform, divergent or convergent rates along these boundaries. The schematic plate boundaries agree to the East Anatolian fault and Bitlis suture zone, the North Anatolian fault in SE Turkey, Bitlis-Zagros fold and thrust belt in Iran and Main Caucasus Trust

fault. The North Anatolian fault (NAF) is dominated by right-lateral strike slip with extension in the Marmara. Along the East Anatolian Fault (EAF) and the Dead Sea Fault (DSF), motions are characterised by left-lateral motion. Arabia-Eurasia convergence is accommodated in the northern Iran and Caucasus.

4.2. Strain rates

In order to characterize the variations of velocity in the Eastern Mediterranean and Caucasus, we calculated the strain rate and rotation rate fields with grid densities. All the parameters were obtained from 100 km × 100 km grid nodes through a least-squares adjustment, as described by Shen et al. (1996). Understanding the active crustal deformation particularly in terms of strain accumulation and the earthquake cycle is important to improve the estimate of the regional earthquake hazard.

The Middle East, Caucasus and Bitlis-Zagros show negative dilation rates, while west Anatolian areas show positive dilatation rates. The result for the thrust fold is consistent with the rates of GPS shortening. According to Reilinger et al. (2006), the Anatolian region showed positive 2D dilatation rate and significant rotation. In the eastern Mediterranean-Middle East, the predominance of recoverable elastic strain is supported by the general agreement between GPS-derived and geologic fault slip rates. Figs. 6 and 7 illustrate the dilatation rate and principle axes rotation. Fig. 7 shows the extension in the direction NW-SE, W-E in West Anatolian and along NAF. The typical extension rate is about 150–199 nstrain/yr. Anatolia displays large coherent regions of rotation bounded by strike-slip faults with the opposite sense of rotation.

In the eastern Mediterranean region, the rotation of Anatolian plate is counterclockwise bordering with a narrow zone of clockwise rotation on the North Anatolian fault. Aktuğ et al. (2013a,b) computed strain rate between 10–100 nstrain/yr in Central Anatolian, mostly below 50 nstrain/yr. We observed extension and compression strain rate in Central Anatolia. Extensional strain rate is adjacent EAF and DSF with approximately 0–100 nstrainn/yr and compression rate is mostly below 50 nstrain/yr.

Horizontal strain rate is decomposed to principal strain axes: contraction and extension axes. The contraction strain rate is higher in Zagros and Caucasus reaching 100–150 nstrain/yr while contraction orientation in Caucasus is along the NE-SW direction. Main Caucasus Thrust is oriented in the S-NE direction (Kadirov et al., 2014) and maximum strain rate observed approximately reaches 200 nstrain/yr. We observed less contraction rate in North part of Iran (0–50 nstrain/yr) but North-East Zagros mountains, Tabriz fault and Chalderan fault shown extensional rate (50–110 nstrain/yr) and principal axes rotation in the N-S direction. Part of the study corresponds to a major tectonic activity between the East Zagros Mountains and Makran subduction zone respective to Arabia-Eurasia convergence. The principal strain axes, rotation and 2D dilatation have been calculated for each grid node from velocity data. Bayer et al. (2006) predicted large clockwise rotation (4–6 Ma^{-1}) along ZMP fault system. From our analysis (Fig. 8) large rotation is clockwise (70–85 nradian) and principal axes remain mostly along N-S. We also observed extensional rate and principal axes in the NE-SW direction. In Zagros-Makran collision zone the strain rate is related to lateral variations (Regard et al., 2004), from a Zagros continental collision zone to Makran subduction zone.

4.3. Relative motions

We have computed the horizontal velocity gradient, which covers Alborz and Kopek Dag and found oblique shortening of Central Alborz (Jackson et al., 2002). Transparence regime of the South Caspian Basin displaces to southwestward with respect to Central Iranian Block. The maximum contraction observed in the Kopek Dag is about 100–194 nstrain/yr in the NE-SW direction. Mostly clockwise rotation is observed in Alborz and Kopek Dag. We also found an anti-clockwise rotation where the contraction is maximal.

East Anatolian Fault (EAF), the Cyprus subduction arc and the left-lateral Dead Sea Fault (DSF) are a triple junctions, which is a

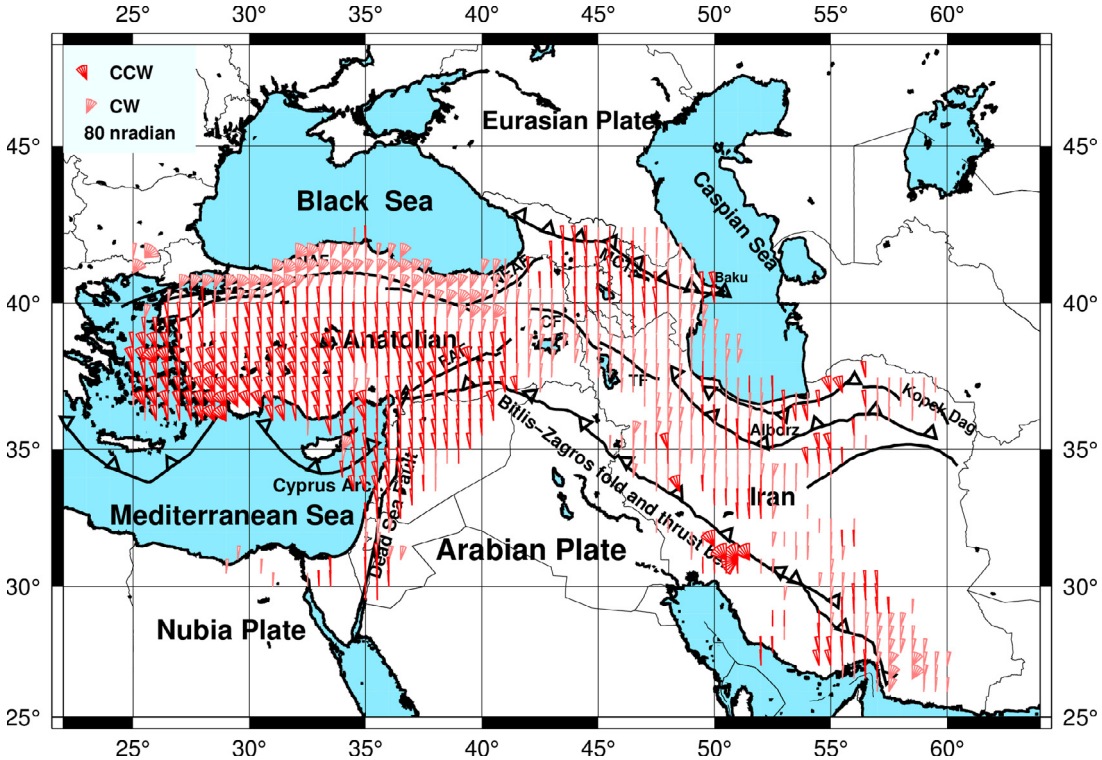

Fig. 8. Map of rotation rates of East Mediterranean and Caucasus.

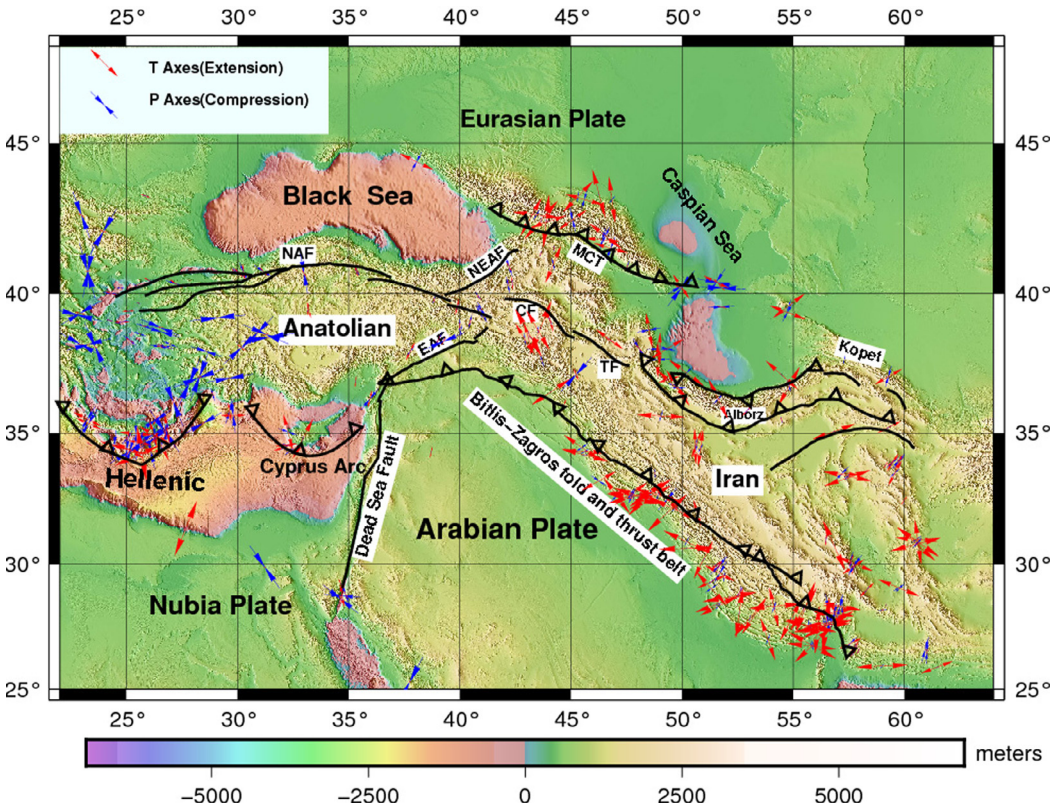

Fig. 9. Horizontal projections of P (in blue) and T (in red) deformation axes derived from the sum of moment tensors (http://ds.iris.edu/spud/momenttensor) with depths ≤35 km.

transform boundary between Arabia and Sinai plates as they converge to Eurasia. Lebanon coast demonstrated SSW motion of Sinai plate relative to Arabia. South of restraining bend, the velocities rotate to a more southward direction, maintaining their fault-parallel orientation (Gomez et al., 2007). The GPS velocities are determined in Syria, along-strike modification from the central and southern DSFS. The extension of Sinai block near the northern end of the DSFS is in the N-S direction in Lebanon and shortening across Palymride fold belt (Alchalbi et al., 2010).

Fig. 7 shows the orientation of shortening and the extension axes in DSFS. According to our results, 2D dilatation did not show any significant change, which is consistent with clear shortening and extension rate in Fig. 6. Extension axe is along N-S and extension rate is up to 100 nstrain/yr (Syria part). The varying pattern of counter clockwise rotation in DSFS is observed. Sinai block shows shortening rate in the range of 0–100 nstrain/yr.

The focal mechanism data are used from Centroid Moment Tensor by Harvard University Catalogue along plate boundary zones. Moment tensors sum of all earthquakes with the depth of smaller than 35 km is shown in Fig. 2. Earthquake focal mechanism was commonly represented by the principal strain axes, i.e., P, T and N axes. In Fig. 9 the horizontal projection of maximum compression of the projections (P) and (T) extension axes shows the principal directions of seismic strain rate. The plate boundary zone is characterised by the relative tectonic regime with T axes in the study area.

4.4. Hazards evaluations

Earthquakes occurred due mainly to deformation or strain accumulation along the plate boundaries. The knowledge of deformation at the surface is important to the description of geodynamics process (strain accumulation) and seismic hazard assessment. Geodetic deformation rate is compared to the earthquake activity rate to assess imbalances and provide insights for future seismic activity. Determination of strain accumulation can identify areas with high seismic hazard. We observed maximum dilatation rate in Western Anatolian. Marmara is a most active region of western Turkey. Historically earthquakes have frequently occurred in this region. Earthquakes at the North Anatolian fault are caused by the northwards motion of the Arabian plate. Also, due to the northwards motion of the African plate this region is in compression, which produces subduction at the Cyprus and Hellenic arcs. The 1999 İzmit earthquake occurred on 17 August in northwestern Turkey. The shock had a moment magnitude of M_w = 7.6, killing around 17,000 peoples and causing approximately half a million people homeless. The 2011 Van earthquake occurred in eastern Turkey near the city of Van. The shock had a moment magnitude of M_w = 7.1 at a shallow depth, causing heavy shaking across much of eastern Turkey and lighter tremors across neighbouring parts of the South Caucasus. The maximal strain is accumulating at present western segments of the North Anatolian Fault. Our results of strain accumulation agree with earthquakes distributions. These results provide direct observations for estimating major earthquakes in the future.

5. Conclusion

The GPS velocity field in the Eastern Mediterranean and Caucasus region reveals the heterogeneous patterns of strain deformation and plates motion. The angular velocities of the Central Iranian, Nubian Plate, Arabian Plate, Anatolian plate and Caucasus block respective to the Eurasia plate are 0.126 ± 0.016 Myr^{-1}, 0.35 ± 0.175 Myr^{-1}, 0.584 ± 0.1 Myr^{-1}, 0.825 ± 0.064 Myr^{-1} and 0.85 ± 0.086 Myr^{-1}, respectively. The counterclockwise rotation is

observed in the Arabian, Anatolian, Aegean regions, Caucasus, adjacent parts of the Zagros and Central Iran and a clockwise rotation is observed in Kavir, Alborz and Lut blocks. Orientation results of relative motion agree with the GPS velocities. Sinai block shows a shortening rate between 0–100 nstrain/yr. Extension is in the N-S direction with rate of 0–100 nstrain/yr. The rotation rate is oriented counter clockwise in DSFS. The maximum contraction is observed in the Kopek Dag with about 100–194 nstrain/yr and directed toward NE-SW. The clockwise and anticlockwise rotations are observed in Alborz and Kopek Dag. The contraction strain rate is about 150–190 nstrain/yr. From our results, the larger rotation is clockwise (70–85 nradian) and principal axes mostly are in N-S direction in the Zagros Mountains and Makran subduction zone. We also observed extensional rate and principal axes along the NE-SW direction. Anatolia displays distinct positive dilatation rate while Middle East, Caucasus and Bitlis-Zagros show negative dilatation rates. West Anatolian and NAF show an extension in the NW-SE and W-E direction. The typical extension rate is about 150–199 nstrain/yr. We observed extensional and compressional strain rate in the Central Anatolian block. The compression rate is below 50 nstrain/yr and extensional strain rate between EAF and DSF south-east of Anatolia remains 0–100 nstrain/yr.

Acknowledgement

Authors would like to thank those who made GPS observations and velocity field available. The figures in this paper were plotted using the public domain Generic Mapping Tools (GMT) software (Wessel and Smith, 1995). This work is supported by the National Natural Science Foundation of China (NSFC) Project (Grant No. 11373059).

References

Afraimovich, E., Ding, F., Kiryushkin, V., Astafyeva, E., Jin, S.G., Sankov, V., 2010. TEC response to the 2008 Wenchuan earthquake in comparison with other strong earthquakes. Int. J. Remote Sens. 31 (13), 3601–3613. http://dx.doi.org/10.1080/01431161003727747.

Aktuğ, B., Meherremov, E., Kurt, M., Özdemir, S., Esedov, N., Lenk, O., 2013a. GPS constraints on the deformation of Azerbaijan and surrounding regions. J. Geodyn. 67, 40–45.

Aktug, B., Nocquet, J.M., Cingöz, A., Parsons, B., Erkan, Y., England, P., Lenk, O., Gürdal, M.A., Kilicoglu, A., Akdeniz, H., Tekgül, A., 2009. Deformation of western Turkey from a combination of permanent and campaign GPS data: limits to block-like behavior. J. Geophys. Res. Solid Earth 114, B10404.

Aktuğ, B., Parmaksız, E., Kurt, M., Lenk, O., Kılıçoğlu, A., Gürdal, M.A., Özdemir, S., 2013b. Deformation of Central Anatolia: GPS implications. J. Geodyn. 67, 78–96.

Alchalbi, A., Daoud, M., Gomez, F., McClusky, S., Reilinger, R., Romeyeh, M.A., Alsouod, A., Yassminh, R., Ballani, B., Darawcheh, R., Sbeinati, R., Radwan, Y., Masri, R.A., Bayerly, M., Ghazzi, R.A., Barazangi, M., 2010. Crustal deformation in northwestern Arabia from GPS measurements in Syria: Slow slip rate along the northern Dead Sea Fault. Geophys. J. Int. 180, 125–135.

Barka, A., Reilinger, R., 1997. Active tectonics of the Eastern Mediterranean region: deduced from GPS, neotectonic and seismicity data. Ann. Geophys. 40 (3), 3892.

Barka, A.A., Kadinsky-Cade, K., 1988. Strike-slip fault geometry in Turkey and its influence on earthquake activity. Tectonics 7, 663–684.

Bayer, R., Chery, J., Tatar, M., Vernant, P., Abbassi, M., Masson, F., Nilforoushan, F., Doerflinger, E., Regard, V., Bellier, O., 2006. Active deformation in Zagros—Makran transition zone inferred from GPS measurements. Geophys. J. Int. 165, 373–381.

DeMets, C., Gordon, R.G., Argus, D.F., 2010. Geologically current plate motions. Geophys. J. Int. 181, 1–80.

DeMets, C., Gordon, R.G., Argus, D.F., Stein, S., 1990. Current plate motions. Geophys. J. Int. 101, 425–478.

DeMets, C., Gordon, R.G., Argus, D.F., Stein, S., 1994. Effect of recent revisions to the geomagnetic reversal time scale on estimates of current plate motions. Geophys. Res. Lett. 21, 2191–2194.

Djamour, Y., Vernant, P., Bayer, R., Nankali, H.R., Ritz, J.-F., Hinderer, J., Hatam, Y., Luck, B., Le Moigne, N., Sedighi, M., Khorrami, F., 2010. GPS and gravity constraints on continental deformation in the Alborz mountain range, Iran. Geophys. J. Int. 183, 1287–1301.

Gomez, F., Karam, G., Khawlie, M., McClusky, S., Vernant, P., Reilinger, R., Jaafar, R., Tabet, C., Khair, K., Barazangi, M., 2007. Global Positioning System measurements of strain accumulation and slip transfer through the restraining bend along the Dead Sea fault system in Lebanon. Geophys. J. Int. 168, 1021–1028. http://dx.doi.org/10.1111/j.1365-246X.2006.03328.x.

Hager, B.H., King, R.W., Murray, M.H., 1991. Measurements of crustal deformation using the Global Positioning System. Annu. Rev. Earth Planet Sci. 19, 351–382.

Herring, T., King, R., McClusky, S., 2006. Global Kalman Filter VLBI and GPS Analysis Program, GLOBK Reference Manual, Release 10.3. MIT, Cambridge, Massachussetts.

Jackson, J., McKenzie, D., 1984. Active tectonics of the Alpine—Himalayan Belt between western Turkey and Pakistan. Geophys. J. Roy. Astron. Soc. 77, 185–264.

Jackson, J., Priestley, K., Allen, M., Berberian, M., 2002. Active tectonics of the South Caspian Basin. Geophys. J. Int. 148, 214–245.

Jin, S.G., Park, P.-H., 2006. Strain accumulation in South Korea inferred from GPS measurements. Earth Planets Space 58, 529–534.

Jin, S.G., Cho, J., Park, J., 2007a. Ionospheric slab thickness and its seasonal variations observed by GPS. J. Atmos. Sol. Terr. Phys. 69 (15), 1864–1870. http://dx.doi.org/10.1016/j.jastp.2007.07.008.

Jin, S.G., Park, P.-H., Zhu, W., 2007b. Micro-plate tectonics and kinematics in Northeast Asia inferred from a dense set of GPS observations. Earth Planet. Sci. Lett. 257, 486–496.

Jin, S.G., van Dam, T., Wdowinski, S., 2013. Observing and understanding the Earth system variations from space geodesy. J. Geodyn. 72, 1–10.

Jin, S.G., Jin, R., Li, J., 2014. Pattern and evolution of seismo-ionospheric disturbances following the 2011 Tohoku earthquakes from GPS observations. J. Geophys. Res. Space Phys. 119 (9), 7914–7927. http://dx.doi.org/10.1002/2014JA019825.

Jin, S.G., Occhipinti, G., Jin, R., 2015. GNSS ionospheric seismology: Recent observation evidences and characteristics. Earth Sci. Rev. 147, 54–64. http://dx.doi.org/10.1016/j.earscirev.2015.05.003.

Kadirov, F.A., Guliyev, I.S., Feyzullayev, A.A., Safarov, R.T., Mammadov, S.K., Babayev, G.R., Rashidov, T.M., 2014. GPS-based crustal deformations in Azerbaijan and their influence on seismicity and mud volcanism, Izvestiya. Phys. Solid Earth 50, 814–823.

Karakhanyan, A., Vernant, P., Doerflinger, E., Avagyan, A., Philip, H., Aslanyan, R., Champollion, C., Arakelyan, S., Collard, P., Baghdasaryan, H., Peyret, M., Davtyan, V., Calais, E., Masson, F., 2013. GPS constraints on continental deformation in the Armenian region and Lesser Caucasus. Tectonophysics 592, 39–45.

King, R., Bock, Y., 2004. Documentation for the MIT GPS Analysis Software: Gamit. Mass. Inst. of Technol, Cambridge.

Koçyiğit, A., Erol, O., 2001. A tectonic escape structure: erciyes pull-apart basin, Kayseri, central Anatolia, Turkey. Geodin. Acta 14, 133–145.

Le Pichon, X., Angelier, J., 1979. The Hellenic arc and trench system: a key to the neotectonic evolution of the eastern Mediterranean area. Tectonophysics 60, 1–42.

Le Pichon, X., Kreemer, C., 2010. The Miocene-to-present kinematic evolution of the Eastern Mediterranean and Middle East and its implications for dynamics. Annu. Rev. Earth Planet. Sci. 38, 323–351. http://dx.doi.org/10.1146/annurev-earth-040809-152419.

Le Pichon, X., Chamot-Rooke, N., Lallemant, S., Noomen, R., Veis, G., 1995. Geodetic determination of the kinematics of central Greece with respect to Europe: implications for eastern Mediterranean tectonics. J. Geophys. Res. Solid Earth 100, 12675–12690.

Mahmoud, S., Reilinger, R., McClusky, S., Vernant, P., Tealeb, A., 2005. GPS evidence for northward motion of the Sinai Block: implications for E. Mediterranean tectonics. Earth Planet. Sci. Lett. 238, 217–224.

Mahmoud, Y., Masson, F., Meghraoui, M., Cakir, Z., Alchalbi, A., Yavasoglu, H., Yonlu, O., Daoud, M., Ergintav, S., Inan, S., 2013. Kinematic study at the junction of the East Anatolian fault and the Dead Sea fault from GPS measurements. J. Geodyn. 67, 30–39.

Masson, F., Anvari, M., Djamour, Y., Walpersdorf, A., Tavakoli, F., Daignières, M., Nankali, H., Van Gorp, S., 2007. Large-scale velocity field and strain tensor in Iran inferred from GPS measurements: new insight for the present-day deformation pattern within NE Iran. Geophys. J. Int. 170, 436–440.

McCaffrey, R., 2002. Crustal block rotations and plate coupling. Plate Boundary Zones, 101–122.

McClusky, S., Balassanian, S., Barka, A., et al., 2000. Global Positioning System constraints on plate kinematics and dynamics in the eastern Mediterranean and Caucasus. J. Geophys. Res. Solid Earth 105, 5695–5719.

McClusky, S., Reilinger, R., Mahmoud, S., Ben Sari, D., Tealeb, A., 2003. GPS constraints on Africa (Nubia) and Arabia plate motions. Geophys. J. Int. 155, 126–138.

McKenzie, D., 1972. Active tectonics of the Mediterranean region. Geophys. J. Int. 30, 109–185.

McKenzie, D., 1978. Active tectonics of the Alpine—Himalayan belt: the Aegean Sea and surrounding regions. Geophys. J. Int. 55, 217–254.

McKenzie, D.P., 1970. Plate tectonics of the Mediterranean region. Nature 226, 239–243.

Nyst, M., Thatcher, W., 2004. New constraints on the active tectonic deformation of the Aegean. J. Geophys. Res. Solid Earth 109, B11406. http://dx.doi.org/10.1029/2003JB002830.

Regard, V., Bellier, O., Thomas, J.C., Abbassi, M.R., Mercier, J., Shabanian, E., Feghhi, K., Soleymani, S., 2004. Accommodation of Arabia-Eurasia convergence in the Zagros-Makran transfer zone, SE Iran: a transition between collision and subduction through a young deforming system. Tectonics 23. TC4007.

Reilinger, R., McClusky, S., Vernant, P., et al., 2006. GPS constraints on continental deformation in the Africa-Arabia-Eurasia continental collision zone and implications for the dynamics of plate interactions. J. Geophys. Res. Solid Earth 111, B05411. http://dx.doi.org/10.1029/2005JB004051.

Reilinger, R.E., McClusky, S.C., Oral, M.B., King, R.W., Toksoz, M.N., Barka, A.A., Kinik, I., Lenk, O., Sanli, I., 1997. Global Positioning System measurements of present-day crustal movements in the Arabia-Africa-Eurasia plate collision zone. J. Geophys. Res. Solid Earth 102, 9983–9999.

Robertson, A., Mountrakis, D., 2006. Tectonic Development of the Eastern Mediterranean Region. Geol. Soci. London Spec. Publ. 260, 1–9.

Shen, Z.-K., Jackson, D.D., Ge, B.X., 1996. Crustal deformation across and beyond the Los Angeles basin from geodetic measurements. J. Geophys. Res. Solid Earth 101, 27957–27980.

Tatar, O., Gürsoy, H., Piper, J.D.A., 2002. Differential neotectonic rotations in Anatolia and the Tauride Arc: palaeomagnetic investigation of the Erenlerda-Volcanic Complex and Isparta volcanic district, south–central Turkey. J. Geol. Soc. 159, 281–294.

Taymaz, T., Eyidogan, H., Jackson, J., 1991. Source parameters of large earthquakes in the east Anatolian fault zone (Turkey). Geophys. J. Int. 106, 537–550.

Tenzer, R., Chen, W., Tsoulis, D., Bagherbandi, M., Sjoberg, L., Novak, P., Jin, S.G., 2015. Analysis of the refined CRUST1.0 crustal model and its gravity field. Surv. Geophys. 36 (1), 139–165. http://dx.doi.org/10.1007/s10712-014-9299-6.

Vernant, P., Chéry, J., 2006. Mechanical modelling of oblique convergence in the Zagros, Iran. Geophys. J. Int. 165, 991–1002.

Vernant, P., Nilforoushan, F., Chery, J., Bayer, R., Djamour, Y., Masson, F., Nankali, H., Ritz, J.F., Sedighi, M., Tavakoli, F., 2004. Deciphering oblique shortening of central Alborz in Iran using geodetic data. Earth Planet. Sci. Lett. 223 (1), 177–185.

Wdowinski, S., Bock, Y., Baer, G., Prawirodirdjo, L., Bechor, N., Naaman, S., Knafo, R., Forrai, Y., Melzer, Y., 2004. GPS measurements of current crustal movements along the Dead Sea Fault. J. Geophys. Res. Solid Earth 109, B05403. http://dx.doi.org/10.1029/2003JB002640.

Wessel, P., Smith, W.H.F., 1995. New version of the generic mapping tools. EOS Trans. Am. Geophys. Union 76. 329-329..

Westaway, R., 1994. Present-day kinematics of the Middle East and eastern Mediterranean. J. Geophys. Res. Solid Earth 99, 12071–12090.